- Technical Paper -

COMPARISON OF ACCELERATED CARBONATION PROCESS OF OPC AND LC^3 UNDER VARYING RELATIVE HUMIDITY CONDITIONS

Luge CHENG[*1], Ryo KURIHARA[*1], Zhenli YANG[*1], Ippei MARUYAMA *[2, *3]

ABSTRACT

This study investigates the carbonation behavior of ordinary Portland cement (OPC) and limestone-calcined clay cement (LC^3) under accelerated carbonation at 30%, 60%, and 90% relative humidity (RH). At 60% RH, vaterite is the predominant carbonation product in both OPC and LC^3. At 90% RH, OPC primarily forms calcite and continues carbonation, whereas LC^3 shows early carbonation cessation due to pore-blocking by tightly nucleated silica gel and calcium carbonate (CC) precipitation, and limited ion transport by the honeycomb-like morphology of C-S-H.

Keywords: LC^3, relative humidity, carbonation

1. INTRODUCTION

The majority of the carbon footprint in the cement industry stems from the decomposition of alkaline carbonates during clinker production. In recent decades, the carbonation of cementitious materials has garnered substantial research attention for its potential to sequester carbon dioxide (CO_2), providing a visible and effective method to partially offset carbon emissions from cement production [1][2]. Recent studies have estimated that the global annual CO_2 uptake through the carbonation of hydrated cement has reached approximately 0.89 Gt by 2019, with cumulative uptake equivalent to 55% of emissions from cement production [3]. In Japan, the annual CO_2 uptake is estimated at 2.6 million tons, accounting for 13.9% of CO_2 emissions generated during cement production [4], highlighting notable variations in carbon sequestration estimations across different regions.

Accurately evaluating the carbon sequestration potential of cementitious materials is essential for leveraging their role in reducing CO_2 emissions. This evaluation necessitates a fundamental investigation of the intrinsic carbonation reactions of cement hydrates, with a particular focus on finely powdered samples to eliminate the influence of mass transport phenomena of gas and liquid present in bulk materials [5].

Limestone calcined clay cement (LC^3) has emerged as a promising alternative to conventional ordinary Portland cement (OPC), combining limestone and calcined kaolinitic clays. LC^3 can replace up to 50% of OPC while maintaining comparable mechanical strength and exhibiting enhanced resistance to chloride penetration and alkali-silica reactions [6][7]. Given its potential for widespread application, it is essential to investigate the carbon capture potential of LC^3 under diverse environmental conditions to better understand its contribution to CO_2 sequestration and sustainability.

This study investigates the carbonation behavior of OPC and LC^3 under accelerated carbonation conditions at low, medium, and high relative humidity (RH). Key aspects analyzed include carbonation rates, calcium carbonate (CC) polymorphs, and the carbonation degree of various hydration products. To minimize the influence of CO_2 transport within the bulk material, finely powdered OPC and LC^3 samples were used. The mineralogical evolution and phase assemblage of hydration products were characterized using X-ray diffraction (XRD) and Fourier-transform infrared spectroscopy (FT-IR). The results elucidate the key hydration products and the structural changes in C-S-H phases, providing valuable insights into the carbonation mechanism of OPC and LC^3 under varying RH conditions.

2. EXPERIMENT METHODS

2.1 Materials and Specimen Preparation

Table 1 Chemical Compositions (%) of the raw materials in OPC and LC^3

Material	CaO	SiO_2	Al_2O_3	Fe_2O_3	MgO	K_2O	Na_2O	SO_3	Cl
Cement	64.19	19.86	5.55	2.80	1.41	0.41	0.28	2.70	0.02
Metakaolin	0.02	50.21	47.01	0.47	0.00	0.13	0.32	0.04	0.01
Limestone	90.24	3.16	0.74	0.74	0.65	0.07	0.00	0.04	0.01
Quartz	0.23	95.20	2.08	1.01	0.26	0.49	0.15	0.28	0.00
Gypsum	43.51	0.45	0.28	0.49	0.38	0.02	0.00	54.38	0.18

*1 Dept. of Architecture, the University of Tokyo, JCI Member
*2 Prof., Dept. of Architecture, the University of Tokyo, JCI Member
*3 Visiting Prof., Dept. of Environmental Engineering and Architecture, Nagoya University, JCI Member

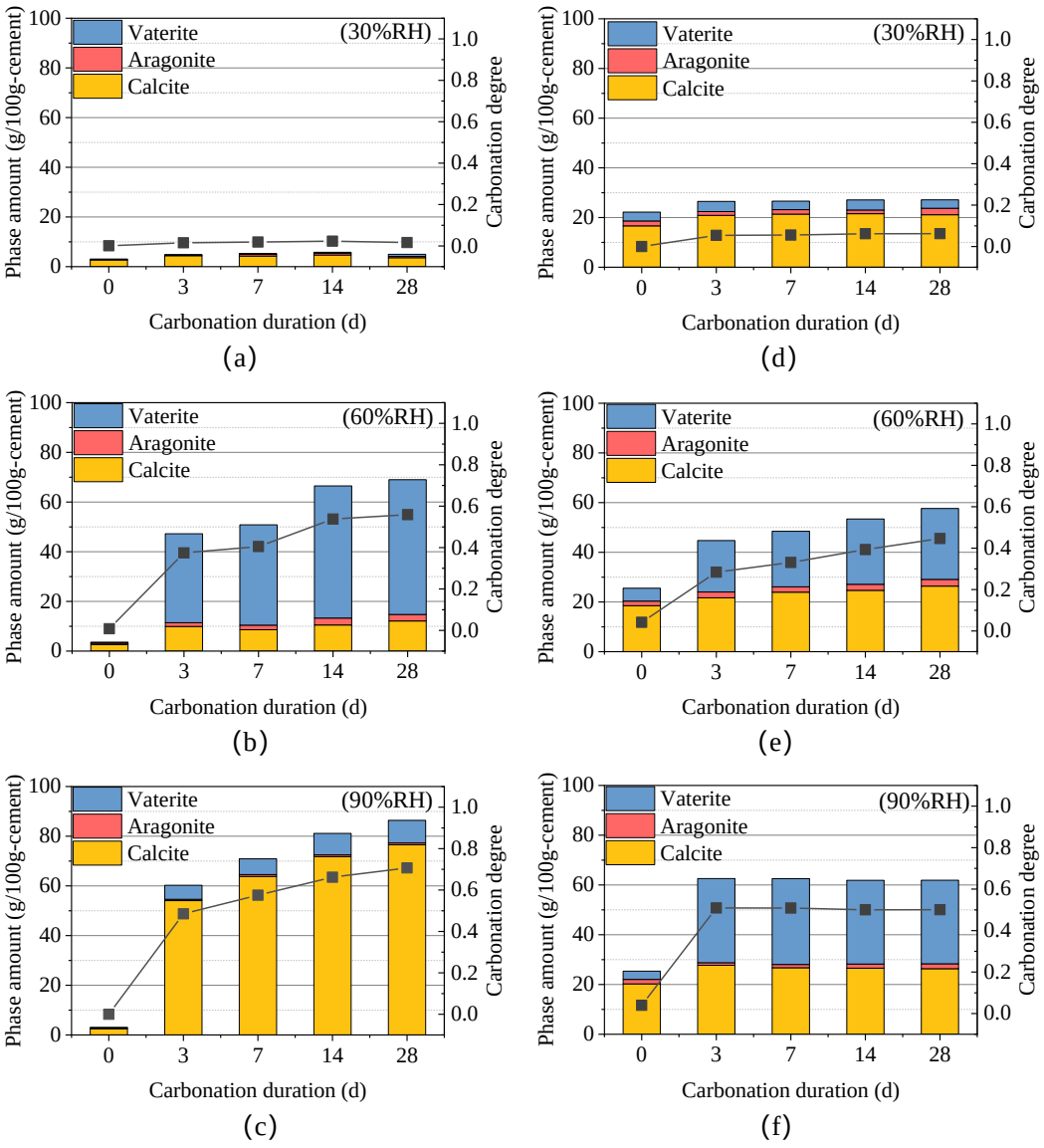

Fig. 1 Amount of CC polymorphs in OPC (a)-(c), and LC^3 (d)-(f) under each RH during carbonation period

Two binder types were investigated: OPC (Mitsubishi UBE Co., Ltd.) and LC^3. The LC^3 was composed of 50% OPC,30 % calcined clay, 15% limestone, and 5% gypsum. The calcined clay consisted of 75% metakaolin (BASF MetaMax®) and 25 % quartz (UBE Co. Ltd., grade 7). The chemical compositions of the raw materials, as measured by X-ray fluorescence (XRF) are detailed in Table 1.

A planetary mixer (ARE-500, THINKY) operating at 1000 rpm was used to achieve a water-to-binder ratio (W/B) of 0.55 for both OPC and LC^3 pastes. The deionized water used for mixing was maintained at 20 ℃ for one day before use. For the OPC paste, water was added in two stages: an initial addition to reach a W/B ratio of 0.30, followed by stirring at 1000 rpm for 1.5 min to ensure homogeneity. The remaining water was then added to achieve the target W/B ratio of 0.55, followed by an additional 1.5 minutes of mixing. After mixing, the fresh cement paste was placed into 500 mL polypropylene bottles and rotated on a roller (IKA ROLLER 10 digital) at 60 rpm for 3.5 h to minimize bleeding and segregation. For the LC^3 paste, gypsum was pre-dissolved in water to mitigate the rapid setting of the mixture. The cement, limestone, metakaolin, and quartz were pre-mixed for 10 minutes to ensure homogeneity before water addition. The entire mixture was stirred at 1000 rpm for 1.5 minutes to reach the desired consistency.

The mixed pastes were sealed and cured for over six months at 20 °C to ensure sufficient hydration. After curing, the bulk samples were ground to a powder with particle sizes below 75 μm using a zirconia cup mill. The ground samples were stored for 28 days in an airtight desiccator at 20 °C, with specific relative humidity (RH) levels maintained by saturated salt solutions: 30% RH (saturated CH_3CO_2K solution), 60% RH (saturated NaBr solution), and 90% RH (saturated $BaCl_2$ solution). Following the 28-day RH-controlled preconditioning, the samples were transferred to carbonation incubators (AS ONE) with a constant temperature of 20 °C and a CO_2 concentration of 5%. The RH conditions in the carbonation incubators were controlled using the same

saturated salt solutions employed during the drying process, maintaining environments of 30%, 60%, and 90% RH.

2.2 Method

During the carbonation period, X-ray diffraction (XRD) analysis was conducted to investigate the mineralogical evolution and quantify the crystalline phases in the samples. The analysis was conducted using a PANalytical Empyrean diffractometer equipped with Cu Kα radiation. The measurements were carried out over a 2θ range of 5°–70°, with a step size of 0.026° and a scanning rate of 0.026°/s. Rietveld refinement was applied using the TOPAS software to determine the quantitative phase composition. The analysis employed an external standard method, with corundum crystal used as the reference standard to enhance accuracy in phase quantification.

Fourier-transform infrared spectroscopy (FT-IR) was employed to analyze the structural changes in C-S-H during the carbonation process. The measurements were conducted using a Bruker ALPHA II spectrometer, with a resolution of 2 cm^{-1} over a wavenumber range of 350 to 4000 cm^{-1}. To ensure high precision and reliability, each spectrum was obtained as an average of 128 integrations.

3. RESULTS

3.1 X-ray diffraction/Rietveld analysis

The quantification results of calcium carbonate (CC) crystalline phases (calcite, vaterite, and aragonite) during the carbonation period are present in Fig. **1**. Additionally, the total carbonation degree (α) was calculated and shown, using the equation presented in Eq. (1).

$$\alpha = \frac{(m_{CC} - m_{CC}^0) \cdot \frac{M_{CaO}}{M_{CC}}}{(1 - LOI) \cdot m_{CaO}^0}, \quad (1)$$

where m_{CC}^0 and m_{CC} are the calcium carbonate contents in the non-carbonated and carbonated samples, respectively; m_{CaO}^0 is the calcium oxide content in the cement before carbonation, which is 64.19%; M_{CaO} and M_{CC} represent the molar masses of CaO (56 g/mol) and $CaCO_3$ (100 g/mol), respectively; LOI represents the ratio of water loss upon ignition.

Under the 30% RH condition (Fig. 1 (a) and (d)), neither OPC nor LC^3 exhibits significant carbonation, which is consistent with expectations due to limited availability of water to dissolve CO_2. It should be noted that the presence of calcite in LC^3 originates from the added limestone. In contrast, under the 60% RH condition, vaterite emerges as the predominant CC phase during the carbonation process for both OPC and LC^3. The carbonation degree, corresponding to the total amount of CC phases, increases gradually with the carbonation duration for both materials. For OPC, the carbonation degree reaches its maximum value of 0.53, while for LC^3, the highest carbonation degree observed

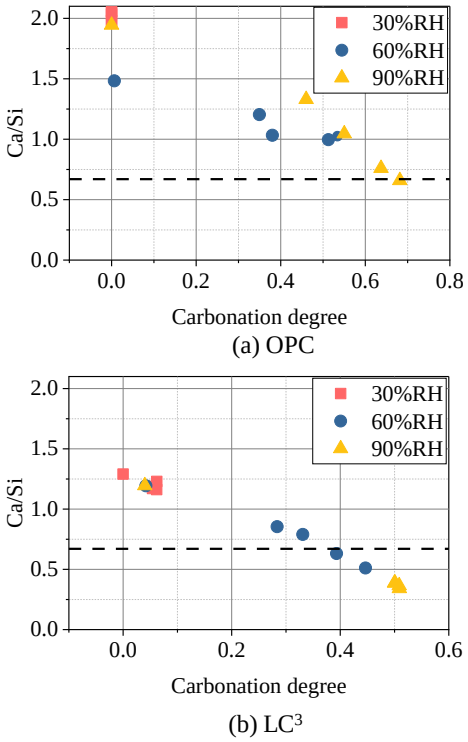

(a) OPC

(b) LC^3

Fig. 2 Relationship between Ca/Si ratio and carbonation degree

is 0.45.

Under the 90% RH condition, OPC and LC^3 exhibit distinct carbonation behaviors. In OPC, the predominant CC phase is calcite, while vaterite emerges as the predominant CC phase in LC^3. The carbonation degree of OPC and LC^3 shows significant increases at the early carbonation stage (3 days). For OPC, the carbonation rate slows thereafter, gradually increasing until 28 days, reaching a value of 0.68. Interestingly, in LC^3, carbonation progress halts after 3 days, with the carbonation degree remaining constant at 0.51 until 28 days.

The Ca/Si ratio of C-S-H was determined using the mass balance method described in [10] based on XRD/Rietveld quantification results. The relationship between the Ca/Si and carbonation degree in OPC and LC^3 is present in Fig. 2, revealing a linear correlation for both materials. Reportedly, the minimum allowable Ca/Si ratio for decalcified tobermorite is 0.67 [11]. Below this threshold, the decomposition of Ca-O sheets in C-S-H occurs, leading to the precipitation and subsequent polymerization of silica gel. Thus, a Ca/Si ratio of C-S-H below 0.67 (indicated by the dashed line in the figures) indicates C-S-H decomposition, while a Ca/Si ratio above 0.67 represents C-S-H decalcification.

From Fig. 2 (a), the initial Ca/Si ratio of non-carbonated OPC is 2.05. Under all carbonation conditions, the Ca/Si ratio of C-S-H exceeds 0.67, ensuring the retention of its layered structure during decalcification. Conversely, in LC^3, with a significantly lower initial Ca/Si ratio of 1.29, Fig. **2** (b) reveals that C-S-H decomposition begins at an early stage of carbonation under 60% and 90% RH conditions: after 7 days for 60% RH and as early as 3 days for 90% RH.

Besides, the carbonation degree of the main hydrates in OPC and LC^3, ettringite (α_{Ett}), portlandite (α_{CH}) and C-S-H ($\alpha_{C\text{-}S\text{-}H}$), are calculated as follows:

$$\alpha_{CH} = (m^0_{CH} - m_{CH})/m^0_{CH} \quad (2)$$

$$\alpha_{Ett} = (m^0_{Ett} - m_{Ett})/m^0_{Ett} \quad (3)$$

$$\alpha_{C-S-H} = (m_{CC} - \frac{m^0_{CH} - m_{CH}}{M_{CH}} \cdot M_{cc} - \frac{m^0_{Ett} - m_{Ett}}{M_{Ett}} \cdot M_{cc} - m^0_{CC})/(a \cdot M_{cc} \cdot \frac{m^0_{CSH}}{M_{CSH}}) \quad (4)$$

where m^0_{CH}, m^0_{Ett}, m^0_{CC}, and m^0_{CSH} are the initial contents of CH, Ett, CC, and C-S-H in the non-carbonated sample, respectively. m_{CH}, m_{Ett}, and m_{CC} are the CH, Ett, and CC content, respectively, detected at each depth. M_{CH}, M_{Ett}, M_{CC}, and M_{CSH} are the molar masses of CH, Ett, CC, and C-S-H, respectively, a is the Ca/Si ratio of C-S-H in the non-carbonated samples.

Fig.3 shows the evolution of the carbonation degree of each hydration product in OPC and LC^3. Ettriginte shows significant decomposition under all RH conditions both in OPC and LC^3, even there is no carbonation reaction under the 30%RH condition, such decomposition is not only due to the carbonation, but also the decomposition by drying process. In OPC under the 60%RH condition, the carbonation of all hydrates increases significantly initially, then increase gradually, at the end of carbonation duration, the carbonation of Ett is almost completely, then the carbonation of CH reaches approximately 0.69, and C-S-H reaches to 0.47. Interestingly, the order of the carbonation degree of CH and Ett inverse under 90% RH, the highest carbonation degree occurs in CH, and reach to the highest value of 0.95, then Ett reach to 0.73, and the smallest carbonation degree is still C-S-H, reach to 0.58. it should be noted that under 60% RH and 90% RH, the carbonation degree of hydration products do not reach to their plateaued

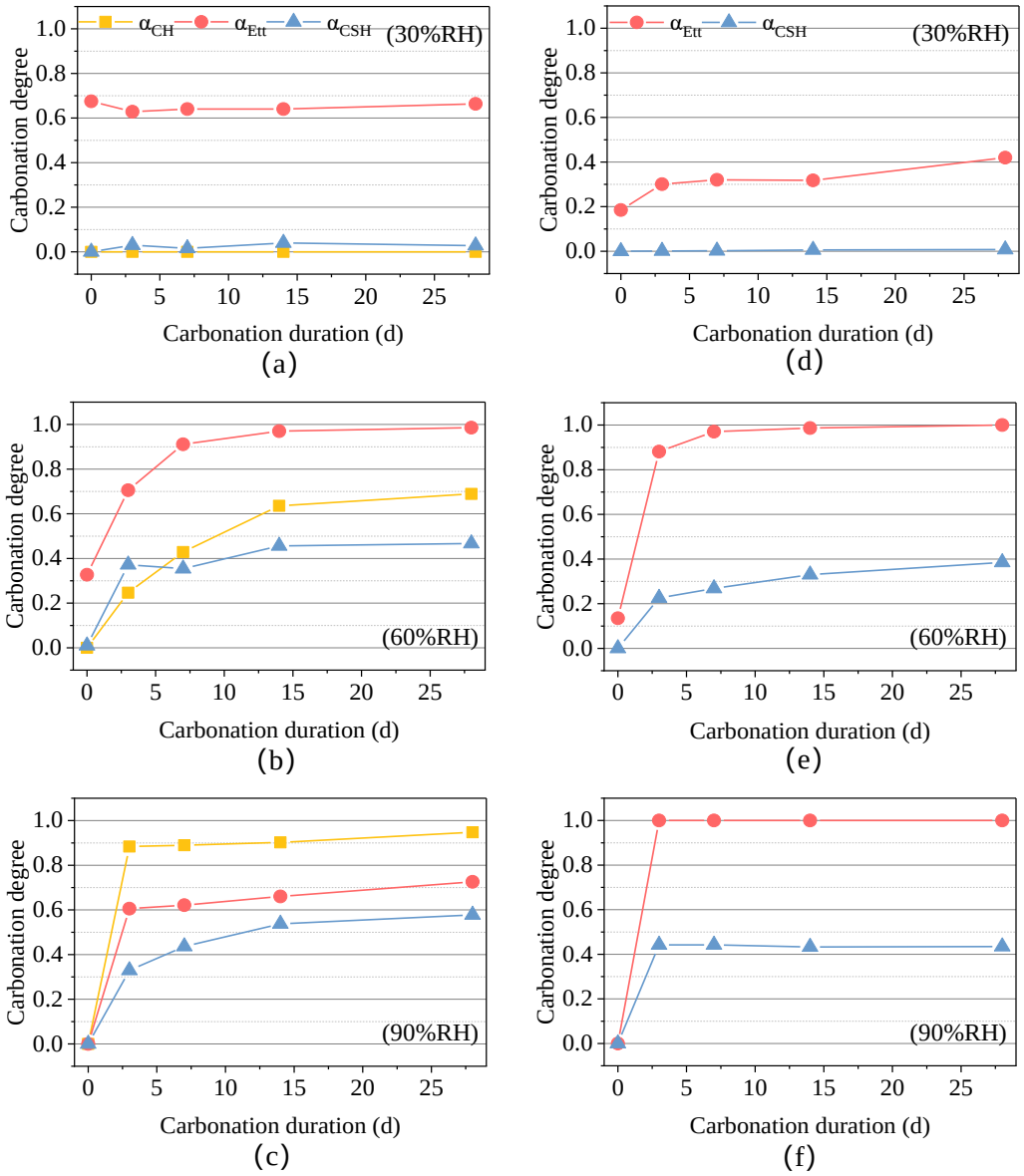

Fig. 3 Carbonation degree of hydration products in OPC (a)-(c), and LC^3 (d)-(f) under each RH during carbonation period

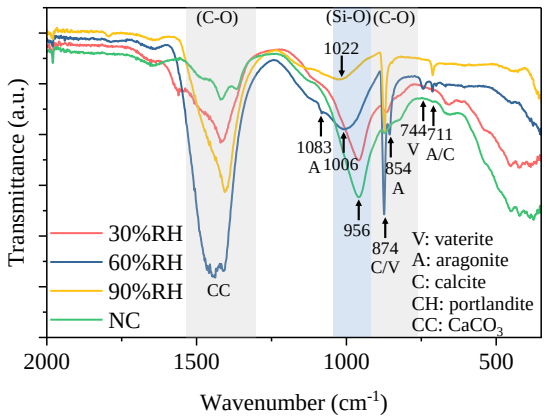

(a) OPC

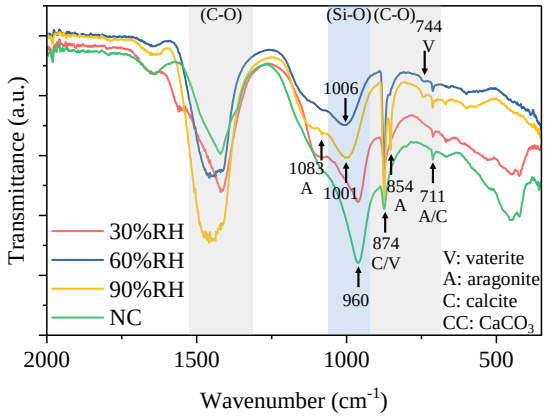

(b) LC^3

Fig. 4 FTIR spectra for OPC(a) and LC^3(b)

state at the end of carbonation duration of 28 days, consistent with the total carbonation degree trend shown in Fig. 1. In LC^3, similar phenomenon can be observed under 60% RH, while under 90% RH, the carbonation degree of both Ett and C-S-H reached to the plateaued at the early age of carbonation duration at 3 days.

3.2 Fourier transform infrared (FTIR) spectroscopy

The FTIR spectra of non-carbonated and carbonated OPC and LC^3 samples during the carbonation period are shown in Fig.4. Under 60% RH, characteristic peaks for aragonite, vaterite, and calcite were observed in OPC at 854, 744 and 874 cm^{-1}, respectively. When under 90% RH, the peaks corresponding to vaterite and aragonite disappeared, with the calcite peak dominating. For LC^3, the vaterite peak persisted under both 60% and 90% RH conditions, reflecting the stabilization of vaterite due to the interaction with fine pores within the C-S-H structure. Additionally, an aragonite peak was observed under 90% RH.

In addition, the structural changes of C-S-H can be inferred from shifts in the Si-O bond within the range of 900 to 1200 cm^{-1} [12]. For both OPC and LC^3, the Si-O bond peaks shifted significantly with increasing RH. In OPC, the peaks moved from approximately 956 cm^{-1} to 1022 cm^{-1}, while in LC^3, a similar shift was observed towards 1022 cm^{-1}. This shift in the Si-O bond , accompanied by a broader peak profile, reflects the progressive decalcification and decomposition of C-S-H as RH increases.

4. DISCUSSION

Vaterite, a metastable CC polymorph, stabilizes in both OPC and LC^3 under 60% RH condition within the fine pores (interlayer and gel pores) between C-S-H layers via strong surface interaction [9]. Under 90% RH condition, OPC and LC^3 exhibit distinct carbonation behaviors due to differences in their hydration products. In OPC, the predominant CC phase is calcite, attributed to its higher CH content, which provides sufficient Ca ions for calcite formation (Fig. 3(c)). Conversely, in LC^3, vaterite emerges as the predominant CC phase, likely resulting from its lower calcium-bearing phases content. This limited CH availability drives extensive carbonation of alternative hydration products, including C-S-H and Ett (Fig. 3(f)), resulting in the stabilization of metastable vaterite within the fine pores nestled between the C-S-H layers.

The different order of the carbonation degree of hydration products in OPC under 60% RH (Ett>CH>C-S-H) and 90% RH conditions (CH>Ett>C-S-H), as shown in Fig. 3 (b) and (c), can be attributed to various in water content. Under 60% RH, the decomposition of Ett is driven by both the carbonation and drying processes, evident from its initial decomposition degree of 0.33 at the first day. The carbonation degrees of CH and C-S-H increase gradually throughout the 28-day carbonation duration. Under 90% RH, where sufficient water is available, Ett decomposition by drying is absent, and the carbonation of all hydration products shows an initial rapid increase followed by a gradual rise until the end of the carbonation period. CH preferentially undergoes carbonation under sufficient water conditions, serving as a buffer for other calcium-bearing phases, including Ett and C-S-H. Similar trends are observed in LC^3 (Fig. 3 (e), (f)).

Interestingly, under 90% RH condition, OPC demonstrates a continuous carbonation process, with the total carbonation degree and the carbonation degrees of individual hydration products increasing steadily until the end of the carbonation period. In contrast, LC^3 exhibits carbonation cessation at an early stage, with the total carbonation degree plateauing at 0.51 after 3 days and remaining constant until 28 days. This discrepancy highlights the impact of hydration product composition and the morphology of C-S-H. The lower carbonation degree of C-S-H in LC^3 compared to OPC can be attributed to the honeycomb-like morphology of C-S-H, which limits ion transport [14], its lower Ca/Si ratio, and the reduced amount of calcium-bearing phases.

In OPC, carbonation causes an enlargement of pore size due to the release of Ca ions from C-S-H layers. The C-S-H retains its tobemorite structure with a Ca/Si above 0.67 (Fig. 2 (a)) under all carbonation conditions, and the release of Ca ions weakens the attractive forces between C-S-H layers, leading to increased layer spacing [15]. This expanded space enables the continuous transport of ions through the fibrillar C-S-H structure, even as the solid volume increases due to the formation

of CC phases.

In LC^3, the rapid decomposition of C–S–H during the early stages of carbonation under 90% RH (Fig. 2(b)) results in the formation of silica gel and calcium carbonate (CC) phases around the particle surfaces within 3 days since the Ca/Si is lower than 0.67 (Fig. 2 (b)), beyond which further carbonation ceases (Fig. 1 (f)). This cessation is likely caused by pore-blocking effects and equilibrium conditions. The tightly nucleated silica gel and CC precipitation within pores effectively block the pore network, significantly reducing the gas-liquid interfacial area for CO_2 dissolution. Additionally, the honeycomb-like morphology of C-S-H with a low Ca/Si ratio in LC^3 further inhibits the dissolution of Ca^{2+} ions from within the particles. These combined factors lead to the cessation of the carbonation process in LC^3 under high RH conditions.

5. CONCLUSIONS

This study compared the carbonation behavior of OPC and LC^3 under accelerated carbonation conditions at low (30%), medium (60%), and high (90%) RH conditions, revealing significant differences in carbonation mechanisms and their dependence on RH.

1) Carbonation products polymorphs: Vaterite stabilizes as the predominant calcium carbonate (CC) polymorph in both OPC and LC^3 under 60% RH due to strong surface interactions within fine pores. Under 90% RH, OPC predominantly forms calcite due to its higher CH content and sufficient water. Conversely, LC^3 primarily forms vaterite, driven by its lower calcium-bearing phase content and extensive carbonation of alternative hydration products like C-S-H and Ett.

2) Distinct carbonation process: OPC shows continuous carbonation under 90% RH, attributed to the retention of a layered tobermorite structure in C-S-H and enlarged pore sizes that support ion transport. In contrast, LC^3 experiences carbonation cessation at an early stage due to pore-blocking by tightly nucleated silica gel and CC precipitation, reduced gas-liquid interfacial areas for CO_2 dissolution, and the ion transport limitations of its honeycomb-like C-S-H morphology.

ACKNOWLEDGEMENT

This study was based on the results obtained from a project (JPNP21023) commissioned by the New Energy and Industrial Technology Development Organization (NEDO).

REFERENCES

[1] H. El-Hassan and Y. Shao, “Carbon Storage through Concrete Block Carbonation,” *J. Clean Energy Technol.*, vol. 2, no. 3, pp. 287–291, 2014.

[2] D. P. Siriwardena and S. Peethamparan, “Quantification of CO2 sequestration capacity and carbonation rate of alkaline industrial byproducts,” *Constr. Build. Mater.*, vol. 91, pp. 216–224, Aug. 2015.

[3] R. Guo *et al.*, “Global CO2 uptake by cement from 1930 to 2019,” *Earth Syst. Sci. Data*, vol. 13, no. 4, pp. 1791–1805, Apr. 2021.

[4] D. Sawa, N. Yamashita, H. Tanikawa, I. Daigo, and I. Maruyama, “CO2 uptake estimation in Japan’s cement lifecycle,” *J. Clean. Prod.*, vol. 486, no. December 2024, p. 144542, Jan. 2025.

[5] N. Saeki *et al.*, “Natural carbonation process in cement paste particles in different relative humidities,” *Cem. Concr. Compos.*, vol. 146, no. December 2023, p. 105400, 2024.

[6] F. Zunino and K. Scrivener, “Microstructural developments of limestone calcined clay cement (LC3) pastes after long-term (3 years) hydration,” *Cem. Concr. Res.*, vol. 153, no. December 2021, p. 106693, Mar. 2022.

[7] K. Scrivener, F. Martirena, S. Bishnoi, and S. Maity, “Calcined clay limestone cements (LC3),” *Cem. Concr. Res.*, vol. 114, no. March 2017, pp. 49–56, 2018.

[8] A. C. A. Muller, K. L. Scrivener, A. M. Gajewicz, and P. J. McDonald, “Densification of C–S–H Measured by 1 H NMR Relaxometry,” *J. Phys. Chem. C*, vol. 117, no. 1, pp. 403–412, Jan. 2013.

[9] T. Uno *et al.*, “Understanding Carbonation Phenomenon of C-S-H through Layer Structure Changes and Water Exchange,” 2024.

[10] I. Maruyama and G. Igarashi, “Cement reaction and resultant physical properties of cement paste,” *J. Adv. Concr. Technol.*, vol. 12, no. 6, pp. 200–213, 2014.

[11] J. J. Chen, J. J. Thomas, and H. M. Jennings, “Decalcification shrinkage of cement paste,” *Cem. Concr. Res.*, vol. 36, no. 5, pp. 801–809, May 2006.

[12] P. Yu, R. J. Kirkpatrick, B. Poe, P. F. McMillan, and X. Cong, “Structure of Calcium Silicate Hydrate (C-S-H): Near-, Mid-, and Far-Infrared Spectroscopy,” *J. Am. Ceram. Soc.*, vol. 82, no. 3, pp. 742–748, Mar. 1999.

[13] F. D’Orazio, J. C. Tarczon, W. P. Halperin, K. Eguchi, and T. Mizusaki, “Application of nuclear magnetic resonance pore structure analysis to porous silica glass,” *J. Appl. Phys.*, vol. 65, no. 2, pp. 742–751, 1989.

[14] L. Cheng *et al.*, “Plugging effect of fine pore water in OPC and LC3 paste during accelerated carbonation monitored via single-sided nuclear magnetic resonance spectroscopy,” *Cem. Concr. Res.*, vol. 186, no. September, p. 107688, Dec. 2024.

[15] M. Segawa, R. Kurihara, A. Aili, G. Igarashi, and I. Maruyama, “Shrinkage reduction mechanism of low Ca/Si ratio C-A-S-H in cement pastes containing fly ash,” *Cem. Concr. Res.*, vol. 186, no. June, p. 107683, Dec. 2024.